

High-Quality Submicron Nb/Al-AlO_x/Nb Josephson Junctions for Quantum Devices

Ch Kaiser¹, J M Meckbach¹, K Ilin¹, J Lisenfeld², R Schäfer^{3,4},
A V Ustinov^{2,4} and M Siegel^{1,4}

¹Institut für Mikro- und Nanoelektronische Systeme, Karlsruher Institut für Technologie (KIT), Hertzstraße 16, D-76187 Karlsruhe, Germany

²Physikalisches Institut, Karlsruher Institut für Technologie (KIT), Wolfgang-Gaede-Str. 1, D-76131 Karlsruhe, Germany

³Institut für Festkörperphysik, Karlsruher Institut für Technologie (KIT), Hermann-von-Helmholtz-Platz 1, D-76344 Eggenstein-Leopoldshafen, Germany

⁴Center for Functional Nanostructures, Karlsruher Institut für Technologie (KIT), Wolfgang-Gaede-Straße 1a, D-76128 Karlsruhe, Germany

E-mail: christoph.kaiser@kit.edu

Abstract.

We have developed a combined photolithography / electron-beam lithography fabrication process for sub- μm to μm -size Nb/Al-AlO_x/Nb Josephson junctions of high quality. In order to define the junction size precisely and protect its top electrode during anodic oxidation, the novel concept of an aluminum hard mask has been developed and used. Josephson junctions of sizes down to $0.5 \mu\text{m}^2$ have been fabricated and thoroughly characterized. We find that they have a very high quality, which is shown by the IV curves with quality parameters $V_m > 50 \text{ mV}$ at 4.2 K , as well as $I_c R_N$ products of $1.75 - 1.93 \text{ mV}$ attained at lower temperatures. In order to test the usability of our fabrication process for quantum devices, we have also designed, fabricated and experimentally investigated superconducting phase qubits. We found relaxation times $T_1 = 26 \text{ ns}$ and dephasing times $T_2 = 21 \text{ ns}$, which is longer than for similar Nb/AlO_x/Nb qubit structures fabricated by other groups. By investigating the subgap leakage of some Josephson junctions in detail, we found that our coherence times are not limited by quasiparticle leakage.

PACS numbers: 85.25.Dq, 85.25.-j, 85.25.Hv

1. Introduction

Nb/Al-AlO_x/Nb Josephson junctions (JJs) with sizes in the sub- μm to μm range are required or advantageous for many applications such as high-speed superconducting digital circuits, mm-wave receivers and submillimeter wave mixers, programmable voltage standards, SQUIDS and superconducting qubits. Considering the multitude of possible applications, it is not surprising that several fabrication techniques for sub- μm to μm -size junctions have been developed over the years. While a precise and reproducible definition of the JJ size is routinely performed with the help of electron-beam lithography, the application of anodic oxidation in such processes remains a challenge. This is due to the fact that the Nb₂O₅ layer formed during the anodic oxidation creeps under the resist mask protecting the top electrode of the JJ (this is known as "encroachment" [1, 2]). Even for a plasma hardened resist and an anodization voltage of 20 V, a significant encroachment was still observed [1]. Some groups solve this problem by simply omitting the anodic oxidation or performing it at very low voltages below 10 V [3, 4, 5, 6]. Since we found that a certain Nb₂O₅ thickness is needed to ensure low subgap leakage currents, this was not an option for us. Other groups have replaced the resist mask with an insulating hard mask such as SiO or SiO₂ [2, 7, 8, 9, 10], which entirely eliminates the encroachment. These hard masks have to be removed by an additional process step, either by reactive ion etching (RIE) through the insulator right above the JJ or by chemical mechanical polishing (CMP). However, it has been found that plasma processes [11] as well as CMP [12] can damage the Josephson junctions. Furthermore, it is being discussed that such processes might degrade the Nb surfaces and lead to the formation of spurious two-level systems (TLS), which limit the coherence times in superconducting phase qubits [13, 14]. Consequently, we have developed a novel method using an aluminum hard mask, which can be removed by a fast wet etching process with KOH, which does not alter the Nb surfaces and should not damage the Josephson junctions.

This article is organized in four sections: First, the newly developed process is discussed in some detail. Second, we present characteristic measurements, which show the high quality of our Josephson junctions for all discussed applications. Afterwards, we present measurements on phase qubits and evaluate the experimentally observed coherence times, in order to see if our process is suitable for the fabrication of quantum devices. Finally, possible decoherence mechanisms in our technology are discussed.

2. Fabrication Process

As a first step in the fabrication, Nb/Al-AlO_x/Nb trilayers are deposited *in-situ* on an oxidized silicon substrate in a vacuum system containing Nb and Al magnetron sputtering targets. Both Nb films are 100 nm thick and are DC sputtered at a power of $P = 300$ W in the main chamber of our two-chamber vacuum system. Special care has been taken to achieve stress-free Nb films. This was done by systematically varying

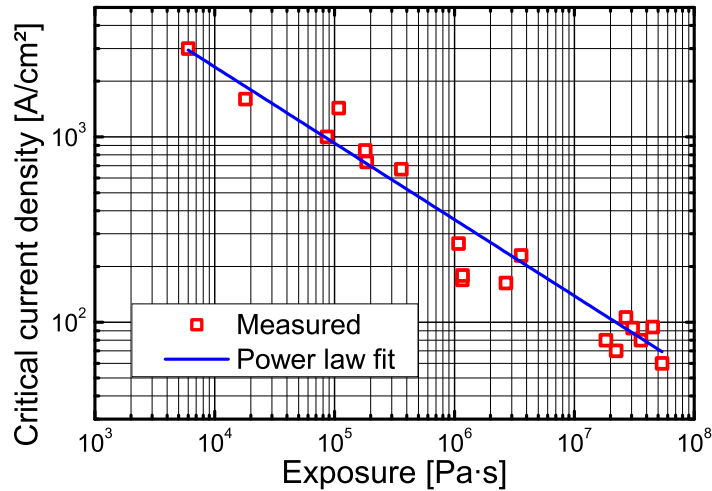


Figure 1. Critical current density of our JJs as a function of the oxygen exposure during the formation of the tunneling barrier.

the Ar working pressure for a Nb film thickness of 200 nm. Subsequently, the curvature of the silicon substrate bending under the film stress was measured. For the optimal working point, residual resistance ratios (RRR) of 4 and transition temperatures of $T_c = 9.2$ K were obtained on 250 nm thick films, confirming the expected high quality of the Nb electrodes. Furthermore, the Nb films showed excellent microwave properties and were used for the fabrication of resonators with high quality factors [15, 16]. The tunneling barrier is formed by DC sputtering of a 7 nm thick Al layer at $P = 100$ W and a subsequent oxidation of this layer in the load lock of the deposition system. This oxidation is performed at room temperature in pure oxygen for 30 min. The critical current density of the Josephson junctions can be reliably controlled in a wide range by the O_2 pressure during oxidation (see Figure 1), so that the required parameters can be achieved for a multitude of applications. Afterwards, the shape of the bottom electrode (including the alignment marks for the following electron-beam lithography) is defined by positive photolithography. After this, the trilayer is patterned by subsequent reactive ion etching ($\text{CF}_4 + \text{O}_2$), Ar ion beam etching (IBE) and again RIE.

In the following, the Josephson junctions are defined with the use of a hard mask. As already discussed, we wanted to avoid any further processes which might damage the junctions or alter the Nb surfaces such as plasma etching or CMP. Hence, insulators like SiO or SiO_2 were ruled out as hard mask material. To find an alternative, we searched for a metal that could be anodized, so that it would not act as a shortcut for the anodization current, and that could be removed selectively by a clean wet etching process. Since aluminum fulfills all of these criteria, the hard mask is created by positive electron-beam lithography and DC sputtering of a 50 nm thick Al layer with subsequent lift-off. It is then used for patterning of the junctions, which begins with etching the top electrode of the trilayer by RIE. Since aluminum is not etched here, both the AlO_x tunneling barrier and the Al mask act as ideal etch stoppers. Now, the first insulating

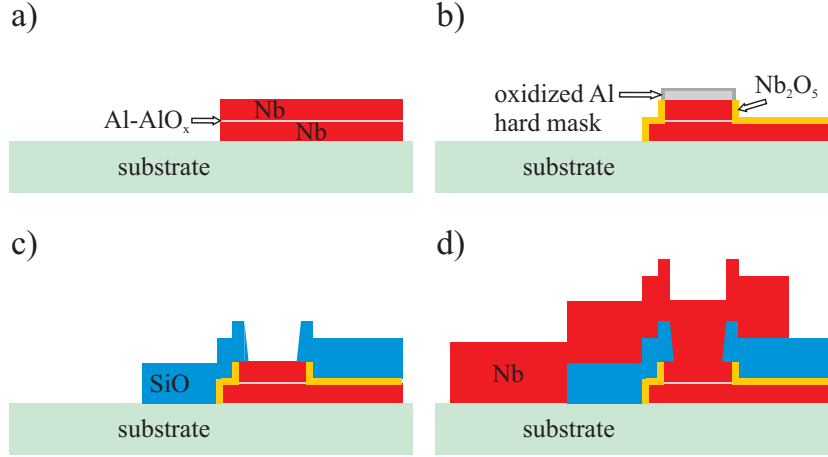


Figure 2. Schematic overview of the JJ fabrication process. a) After deposition and patterning of the trilayer. b) After JJ definition and anodic oxidation. c) After removal of the hard mask and deposition of the SiO insulation layer. d) Final structure after definition of the wiring layer.

layer is formed by anodic oxidation of the samples. Here, it is taken care that all sidewalls of the lower trilayer electrode are oxidized. The anodization takes place in an aqueous solution of $(\text{NH}_4)\text{B}_5\text{O}_8$ and $\text{C}_2\text{H}_6\text{O}_2$ at room temperature. Per applied volt, 0.88 nm Nb are turned into 2.3 nm Nb_2O_5 and 0.9 nm Al are turned into 1.3 nm AlO_x [17], so that for a typical anodization voltage of 25 V, only half the thickness of the Al hard mask is oxidized and the underlying Nb is protected. The hard mask is removed by wet etching with KOH, which does not alter the Nb surface and should not damage the Josephson junctions.

After that, the second insulator SiO is deposited employing positive e-beam lithography, thermal evaporation and lift-off. During evaporation, the wafers are water cooled in order to avoid thermally induced damage to the resist. Finally, the Nb wiring layer is defined by negative photolithography and deposited in a magnetron sputtering system. Here, an *in-situ* pre-cleaning by low-energy Ar IBE is carried out before the sputtering, in order to provide a good electrical contact between the top junction electrode and the wiring layer. This is especially required for JJs sizes in the sub- μm range where the aspect ratios of the vias through the SiO layer come close to one. An overview of the entire fabrication process can be found in Figure 2.

3. JJ Characterization

We have fabricated junctions of various critical current densities j_c and characterized them at 4.2 Kelvin. One important quality parameter is the ratio of subgap resistance R_{sg} (evaluated at a voltage of 2 mV) over normal resistance R_N . For the entire range of critical current densities shown in Figure 1, this R_{sg}/R_N ratio was typically larger than 30, which indicates a very high quality. Other important quality parameters like the $I_c R_N$ product or the characteristic voltage $V_m = I_c R_{\text{sg}}$ require the measurement of the

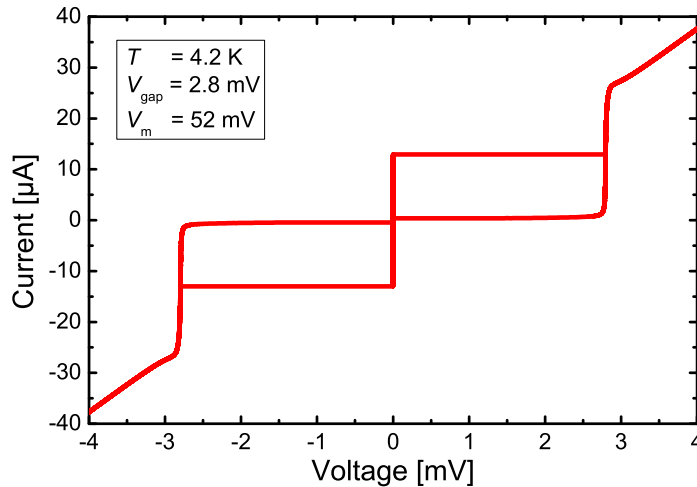


Figure 3. IV curve of a circular junction with an area of $0.5 \mu\text{m}^2$ and a critical current density of $j_c = 3 \text{ kA}/\text{cm}^2$, measured at 4.2 Kelvin.

critical current I_c . For μm -size junctions of low critical current densities, the critical currents $I_c < 10 \mu\text{A}$ are strongly suppressed at $T = 4.2 \text{ K}$ due to thermal noise, so that $I_c R_N$ and V_m values could not be determined.

In order to still get information about these parameters, we fabricated a batch of samples with $j_c = 3 \text{ kA}/\text{cm}^2$; the IV curve of a sample with an area of $0.5 \mu\text{m}^2$ can be seen in Figure 3. Although the critical currents I_c in the range of $10 - 20 \mu\text{A}$ were still somewhat suppressed at $T = 4.2 \text{ K}$, we could now perform a more detailed analysis. The recorded gap voltages were all 2.8 mV or higher and the characteristic voltages V_m were all larger than 50 mV . For JJs with areas $> 1 \mu\text{m}^2$, we observed values $V_m \geq 60 \text{ mV}$, which we contribute to a less suppressed I_c . Altogether, the IV measurements at 4.2 K all indicate a very high quality of our Josephson junctions.

For four circular junctions with diameters from 1.9 to $3.8 \mu\text{m}$ and $j_c = 660 \text{ A}/\text{cm}^2$, we have also recorded IV curves at $T = 20 \text{ mK}$, where the critical current of the junctions is not suppressed. Here, the gap voltages were in the range of $V_{\text{gap}} = 2.88 - 2.92 \text{ mV}$. Furthermore, we observed no excess currents and $I_c R_N$ products of $1.75 - 1.93 \text{ mV}$. This shows that we have strong Cooper pair tunneling close to the expected Ambegaokar-Baratoff behavior [18].

4. Characterization of Phase Qubit

The technological process described in this article was employed to fabricate phase qubits, of which one was characterized in a dilution refrigerator. We used a critical current density of $j_c = 65 \text{ A}/\text{cm}^2$ and a standard phase qubit design. All vias necessary for the connection of the wiring to the lower electrode were not realized as large junctions, but the tunneling barrier was etched away with IBE, so that real vias were formed. Schematics and a photograph of the circuit as well as design values can

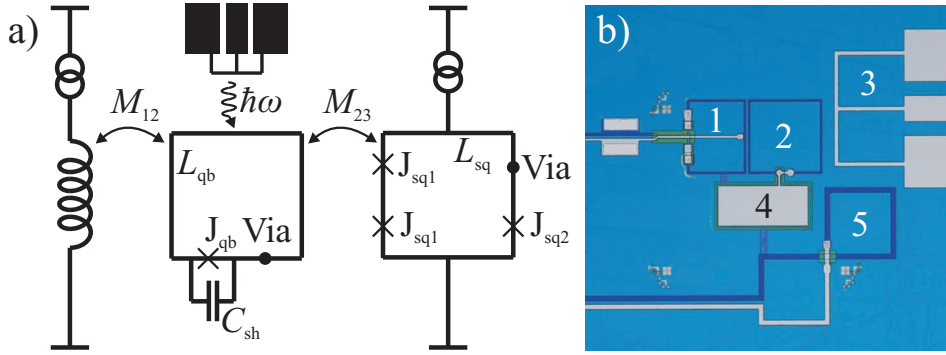


Figure 4. a) Circuit schematics of the phase qubit that was investigated. All junctions are circular and their diameters are given. The designed circuit parameters account for: $d_{J,\text{qb}} = 3.1 \mu\text{m}$, $d_{J,\text{sq1}} = 2.83 \mu\text{m}$, $d_{J,\text{sq2}} = 2 \mu\text{m}$, $C_{\text{sh}} = 0.82 \text{ pF}$, $L_{\text{qb}} = 257 \text{ pH}$, $L_{\text{sq}} = 227 \text{ pH}$, $M_{12} = 1.36 \text{ pH}$, $M_{23} = 22 \text{ pH}$. b) Photograph of the same structure with 1 = SQUID, 2 = Qubit, 3 = MW line, 4 = C_{sh} , 5 = Bias coil.

be found in Figure 4. The design values lead to a characteristic qubit parameter of $\beta_L = 2\pi L_{\text{qb}} I_{c,\text{qb}} / \Phi_0 \simeq 3.8$.

The setup and procedure of the measurement have been successfully used for phase qubit investigations before and are described elsewhere [19]. The qubit is read out by application of a short (1 ns) DC flux pulse, during which one magnetic flux quantum tunnels into the qubit loop only if the qubit was in the excited state $|1\rangle$. The associated flux signal is detected by the inductively coupled SQUID, which results in two separated SQUID switching current histograms depending on whether the qubit was in the ground state $|0\rangle$ or the excited state $|1\rangle$. These switching histograms could be used to calculate the escape probability P_{esc} , which directly reflects the population of the qubit states. First, by measuring the distance of these two separate SQUID switching peaks and taking into account the slope of the SQUID $I_c(\Phi)$ modulation, we determined the strength of the qubit flux signal in the SQUID to be $\Phi_{\text{sq,qb}} = 73 \text{ m}\Phi_0$. This is slightly higher than the expected design value of $\Phi_{\text{sq,qb}} = M_{23} \cdot I_{c,\text{qb}} = 53 \text{ m}\Phi_0$. Such an increase in the qubit signal strength might be due to a higher critical current of the qubit $I_{c,\text{qb}}$ than designed, which goes along well with the fact that also the observed average qubit level splitting $\Delta_{01} \approx 13 \text{ GHz}$ was slightly higher than expected.

In the following, we chose a working point of $\Delta_{01} = 14.48 \text{ GHz}$ to characterize the qubit. To measure Rabi oscillations, we initialized the qubit in the ground state $|0\rangle$, applied a microwave (MW) pulse with increasing length immediately followed by the DC readout pulse. The result is shown in Figure 5a. The oscillations decay exponentially with a characteristic time $T_d = 22.4 \text{ ns}$. The relaxation time T_1 was measured by applying a MW π -pulse, so that the qubit would be brought into the excited state $|1\rangle$, and varying the delay of the readout pulse. We found that our qubit relaxes down to the ground state exponentially with a characteristic time $T_1 = 26 \text{ ns}$. To determine the dephasing time T_2 , we performed a Ramsey-type experiment, in which two $\pi/2$ -pulses separated by a variable duration are applied to the qubit. As expected, the frequency

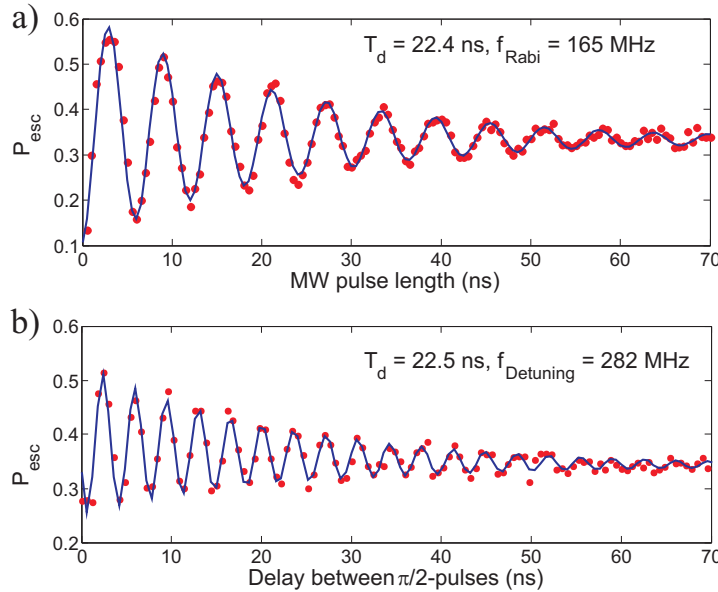


Figure 5. a) Rabi oscillations between the qubit states $|0\rangle$ and $|1\rangle$ at a level splitting of $\Delta_{01} = 14.48$ GHz. b) Ramsey oscillations for a detuning of 282 MHz from this working point.

of the observed Ramsey fringes was equal to the detuning of the microwave from the resonance frequency. An example of such a measurement can be seen in Figure 5b. We determined the decay times of these exponentially decaying oscillations for various detuning values and took the mean value $T_2 = 21$ ns as our dephasing time. This means that we have reached coherence times T_1 and T_2 which are longer than for any other standard design Nb/ AlO_x /Nb phase qubit (for comparison see chapter 5).

5. Discussion of Possible Decoherence Mechanisms

While Al based phase qubits have reached coherence times up to 600 ns [20], for most Nb/Al- AlO_x /Nb phase qubits the relaxation times are shorter than $T_1 \simeq 10$ ns [19, 21, 22, 23] and even the longest observed times do not exceed 20 ns [24, 25, 26]. For all these devices, the dephasing times T_2 could either not be measured or were shorter than the T_1 times. (Only a changed design, in which the phase qubit could be made insensitive to decoherence by operating it at an optimal point, allowed longer coherence times about $T_1 \simeq 100$ ns for a Nb/Al- AlO_x /Nb based device recently [27].) However, a Nb/ AlO_x /Nb process which is suitable for the fabrication of phase qubits would still be desirable since this technology offers big advantages concerning scalability, integrability, reproducibility and yield. Since the coherence times observed in our phase qubit are longer than those in any other Nb/ AlO_x /Nb phase qubit of standard design mentioned above, we tried to learn some more about the reasons of decoherence in our devices.

First, we wanted to make sure that the coherence in our phase qubit was not limited by quasiparticle conductance. A measure for this should be obtainable by the

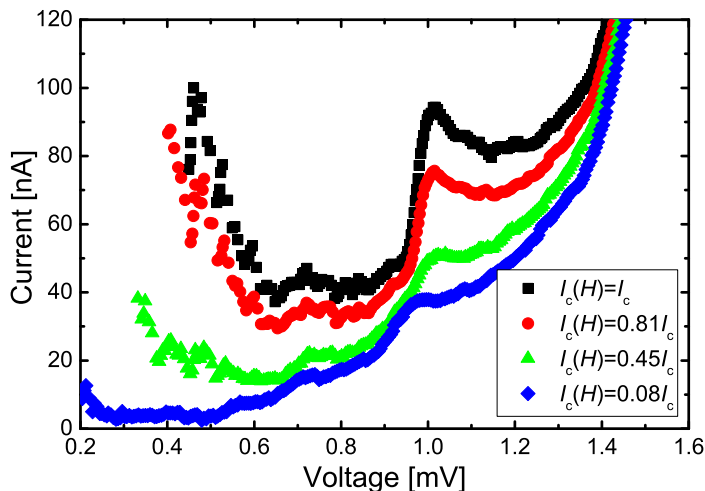


Figure 6. The subgap regime of a circular junction with $d = 3.6 \mu\text{m}$ and $j_c = 660 \text{ A/cm}^2$ for different applied magnetic fields, measured with a voltage bias setup. The subgap leakage current decreases significantly for a more strongly suppressed critical current.

subgap leakage at low voltages V close to retrapping to the zero-voltage state. In the past, voltage bias measurements at mK temperatures with a magnetic field that entirely suppressed the critical current I_c have been used to measure this quasiparticle resistance $R_{\text{sg,max}}$ and use the latter for an estimation of the decoherence rate due to quasiparticle leakage [28, 29].

Consequently, we have measured the subgap regime in a voltage bias setup at various magnetic fields H for four samples with diameters between 1.9 and $3.8 \mu\text{m}$ at $T = 20 \text{ mK}$. Two major current drops at voltages $2\Delta/2$ and $2\Delta/3$ could be seen (see Figure 6) and attributed to Andreev reflections [30]. Below $2\Delta/3$, $R_{\text{sg,max}}$ values could be evaluated at the current minima. We found $R_{\text{sg,max}}/R_N$ ratios at zero magnetic field between $1,160$ and $2,980$, which is in agreement with values of $1,300$ to $1,800$ determined in [29] for samples from different foundries. The data for applied magnetic fields (see Figure 6) show that the attained $R_{\text{sg,max}}$ values increase systematically with a stronger suppression of the critical current. Just as the $R_{\text{sg,max}}/R_N$ ratios at zero field, our dependence of $R_{\text{sg,max}}$ with I_c is in perfect agreement with the data presented in [29]. Unfortunately, due to a limited resolution of our voltage bias setup, we were not able to extend our investigation to the same regime of $I_c(H) = 10^{-4}I_c(0)$ as in [29], so that values for the intrinsic quasiparticle resistance could not be obtained. But since all of our data is in such good agreement with the data reported in [29], we take over their conclusion that the decoherence rate from quasiparticle conductance $1/\tau_{\text{qp}}$ should be as low as $1/\tau_{\text{qp}} = 1/(100 \mu\text{s})$. Although this value is only a rough estimate, we can certainly conclude that the coherence in our phase qubit is not limited by quasiparticle conductance, since τ_{qp} is more than three orders of magnitude larger than our observed coherence times.

It follows that another decoherence mechanism must be present in our phase qubits.

It was discovered recently that the coherence times in phase qubits was limited by the presence of spurious two-level systems (TLS) in their vicinity [13, 14]. The macroscopic manifestation of these TLS are dielectric losses [13, 14]. Since we could rule out decoherence due to quasiparticle conductance, we assume that the presence of such TLS is responsible for our limited coherence times as well as for the decoherence in other Nb/ AlO_x /Nb phase qubits. In the following, we discuss why we might have fewer TLS in our qubits and hence longer coherence times than in similar devices.

TLS have been found in the bulk dielectrics used for insulating layers in qubit fabrication [13] as well as on metal surfaces [31]. We have recently measured the dielectric losses in our Nb_2O_5 and SiO thin films and found them to be rather lossy [32]. Hence, we do not believe that the losses in the insulating layers are responsible for our improved coherence times. Instead, the stronger decoherence in other phase qubits might be due to TLS on the Nb surfaces. This is supported by our recent observation that the TLS responsible for the losses in superconducting coplanar waveguide (CPW) resonators stem from surface or interface states [16]. It seems likely that processes like RIE or CMP alter the Nb surface by ion bombardment, mechanical stress or chemical reaction. Since we have taken care to avoid such processes wherever possible, the enhanced coherence times in our phase qubits might indeed be due to the novel fabrication process presented here. This is supported by the fact that the quality factors of Nb based CPW resonators were found to be significantly larger if the Nb films were lifted-off instead of being patterned by reactive ion etching [33]. However, we still use RIE for trilayer and junction patterning. Consequently, we hope to further increase our T_1 and T_2 times by either improving or entirely omitting our employed RIE process. Additionally, the use of insulating layers with lower dielectric losses should allow for longer coherence times.

6. Conclusions

We have developed a technological process for the fabrication of high quality sub- μm to μm -size Nb/Al- AlO_x /Nb Josephson junctions. This process employs an Al hard mask, which acts as a perfect etch stop for RIE and can be removed by a clean wet etching step. Characterization of our junctions at 4.2 K and mK temperatures showed that we have high quality parameters $V_m > 50$ mV, $V_{\text{gap}} = 2.88 - 2.92$ mV and $I_c R_N = 1.75 - 1.93$ mV. We fabricated phase qubits and characterized one of them at mK temperatures. It exhibited a relaxation time of $T_1 = 26$ ns and a dephasing time of $T_2 = 21$ ns, which is longer than for any other reported Nb/ AlO_x /Nb phase qubit of standard design. By measurements of subgap leakage currents at mK temperatures, we found that decoherence in our phase qubit should not be due to quasiparticle conductance. Hence, we assume that the decoherence is caused by TLS in the qubit vicinity, most likely on the Nb surfaces.

Acknowledgments

This work was partly supported by the DFG Center for Functional Nanostructures, project number B3.4. We also thank H J Wermund, A Stassen and K-H Gutbrod for technical support.

References

- [1] Lee L P S, Arambula E R, Hanaya G, Dang C, Sandell R and Chan H 1991 *IEEE Trans. Magn.* **27** 3133
- [2] Fritzsche L, Elsner H, Schubert M and Meyer H-G 1999 *Supercond. Sci. Technol.* **12** 880
- [3] Ketchen M. B, Pearson D, Kleinsasser A W, Hu C-K, Smyth M, Logan J, Stawiasz K, Baran E, Jaso M, Ross T, Petrillo K, Manny M, Basavaiah S, Brodsky S, Kaplan S B, Gallagher W J and Bhushan M 1991 *Appl. Phys. Lett.* **59** 2609
- [4] Pavolotskya A B, Weimann T, Scherer H, Niemeyer J, Zorin A B and Krupenin V A 1999 *IEEE Trans. Appl. Supercond.* **9** 3251
- [5] Péron I, Pasturel P and Schuster K-F 2001 *IEEE Trans. Appl. Supercond.* **11** 377
- [6] Chen W, Patel V and Lukens J E 2004 *Microelectronic Engineering* **73-74** 767
- [7] Imamura T and Hasuo S 1988 *J. Appl. Phys.* **64** 1586
- [8] Bao Z, Bhushan M, Han S and Lukens J E 1995 *IEEE Trans. Appl. Supercond.* **5** 2731
- [9] Dolata R, Weimann T, Scherer H-J and Niemeyer J 1999 *IEEE Trans. Appl. Supercond.* **9** 3255
- [10] Dolata R, Scherer H, Zorin A B and Niemeyer J 2005 *J. Appl. Phys.* **97** 054501
- [11] Tolpygo S K, Amparo D, Kirichenko A and Yohannes D 2007 *Supercond. Sci. Technol.* **20** S341
- [12] Yamamori H, Yamada T, Sasaki H and Shoji A 2008 *Supercond. Sci. Technol.* **21** 105007
- [13] Martinis J M, Cooper K B, McDermott R, Steffen M, Ansmann M, Osborn K D, Cicak K, Oh S, Pappas D P, Simmonds R W and Yu C C 2005 *Phys. Rev. Lett.* **95** 210503
- [14] McDermott R 2009 *IEEE Trans. Appl. Supercond.* **19** 2
- [15] Hammer G, Wuensch S, Roesch M, Ilin K, Crocoll E and Siegel M 2007 *Supercond. Sci. Technol.* **20** S408
- [16] Macha P, van der Ploeg S H W, Oelsner G, Ilichev E, Meyer H-G, Wunsch S and Siegel M 2010 *Appl. Phys. Lett.* **96** 062503
- [17] Meng X and Van Duzer T 2003 *IEEE Trans. Appl. Supercond.* **13** 91
- [18] Ambegaokar V Baratoff A 1963 *Phys. Rev. Lett.* **10** 486
- [19] Lisenfeld J, Lukashenko A, Ansmann M, Martinis J M and Ustinov A V 2007 *2007* **99** 170504
- [20] Martinis J M 2009 *Quantum Information Processing* **8** 81
- [21] Martinis J M, Nam S and Aumentado J 2002 *Phys. Rev. Lett.* **89** 117901
- [22] Palomaki T A, Dutta S K, Lewis R M, Paik H, Mitra K, Cooper B K, Przybysz A J, Dragt A J, Anderson J R, Lobb C J and Wellstood F C 2007 *IEEE Trans. Appl. Supercond.* **17** 162
- [23] Feofanov A K, Oboznov V A, Bol'ginov V V, Lisenfeld J, Poletto S, Ryazanov V V, Rossolenko A N, Khabipov M, Balashov D, Zorin A B, Dmitriev P N, Koshelets V P and Ustinov A V 2010 *Nature Physics* **6** 593
- [24] Paik H, Dutta S K, Lewis R M, Palomaki T A, Cooper B K, Ramos R C, Xu H, Dragt A J, Anderson J R, Lobb C J and Wellstood F C 2008 *Phys. Rev. B* **77** 214510
- [25] Dutta S K, Strauch F W, Lewis R M, Mitra K, Paik H, Palomaki T A, Tiesinga E, Anderson J R, Dragt A J, Lobb C J and Wellstood F C 2008 *Phys. Rev. B* **78** 104510
- [26] Bennett D A, Longobardi L, Patel V, Chen W and Lukens J E 2007 *Supercond. Sci. Technol.* **20** S445
- [27] Hoskinson E, Lecocq F, Didier N, Fay A, Hekking F W J, Guichard W and Buisson O 2009 *Phys. Rev. Lett.* **102** 097004

- [28] Gubrud M A, Ejrnaes M, Berkley A J, Ramos Jr R C, Jin I, Anderson J R, Dragt A J, Lobb C J and Wellstood F C 2001 *IEEE Trans. Appl. Supercond.* **11** 1002
- [29] Milliken F P, Koch R H, Kirtley J R and Rozen J R 2004 *Appl. Phys. Lett.* **85** 5941
- [30] Arnold G B 1987 *J. Low. Temp. Phys.* **68** 1
- [31] Gao J, Daal M, Vayonakis A, Kumar S, Zmuidzinas J, Sadoulet B, Mazin B A, Day P K and Leduc H G 2008 *Appl. Phys. Lett.* **92** 152505
- [32] Kaiser Ch, Skacel S T, Wünsch S, Dolata R, Mackrodt B, Zorin A and Siegel M 2010 *Supercond. Sci. Technol.* **23** 075008
- [33] Chen W, Bennett D A, Patel V and Lukens J E 2008 *Supercond. Sci. Technol.* **21** 075013